
Yields from single AGB stars

Amanda I. Karakas

Research School of Astronomy & Astrophysics, Mt Stromlo Observatory, Cotter Road, Weston Creek, ACT 2611, Australia akarakas@mso.anu.edu.au

Summary. In order to understand the composition of planetary nebulae we first need to study the nucleosynthesis occurring in the progenitor star during the thermally-pulsing Asymptotic Giant Branch (AGB) phase. I present an overview of single AGB evolution, with an emphasis on the mixing processes that alter the envelope composition, followed by a discussion of the stellar yields available from single AGB stellar models.

Key words: stars: AGB and post-AGB stars, nucleosynthesis, abundances

1 Introduction

The last nuclear burning phase of a low to intermediate-mass (~ 0.8 to $8M_{\odot}$) star's life is the thermally-pulsing asymptotic giant branch (TP-AGB). The outer envelope is lost by low velocity stellar winds during the AGB, with the termination being the final ejection of the envelope. The star then evolves through the brief post-AGB and planetary nebula phases before ending its life as a white dwarf. The gaseous nebula is the remnant of the envelope that once surrounded the core, that is now exposed as the central star of the illuminated nebula. The abundances of the nebula can reveal information about stellar nucleosynthesis and mixing during the AGB. For this reason PN abundances could, in principle, be used to constrain stellar models.

In this proceedings I summarize the evolution and nucleosynthesis during the AGB. I briefly discuss the differences between “synthetic” and “detailed” AGB models, and compare yields from different authors.

2 Asymptotic giant branch stars

The structure and evolution of low and intermediate mass stars prior to and during the AGB has been previously discussed by [5, 11]; see [24] for a review of post-AGB stars. All stars begin their nuclear-burning life on the main sequence. Following core H exhaustion the core contracts, the outer layers expand and the star becomes a red giant, characterized by an inert He core, an H-burning shell, and a deep convective

envelope that extends to the stellar surface. It is during the ascent of the giant branch that the inner edge of the convective envelope moves inward in mass and the first dredge-up (FDU) occurs, where partially H-processed material (e.g. ${}^4\text{He}$, ${}^{13}\text{C}$, ${}^{14}\text{N}$) is mixed to the surface.

After a phase of central He-burning, the core contracts and there is a structural re-adjustment to shell He burning. The re-adjustment drives a strong expansion of the outer layers and the star becomes a red giant for the second time; the star is now said to be on the AGB. For stars with $m \geq 4M_{\odot}$ the convective envelope moves inward to regions where complete H burning (mostly ${}^4\text{He}$ and ${}^{14}\text{N}$) had previously occurred, this is the second dredge up (SDU).

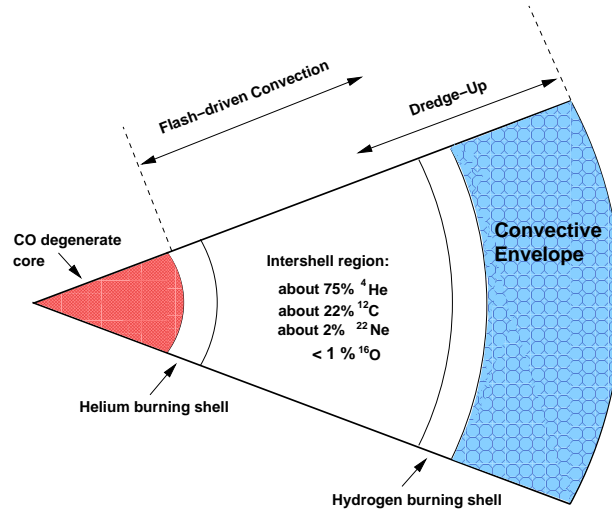


Fig. 1. Schematic structure of an AGB star.

An AGB star is characterized (Fig. 1) by two nuclear burning shells, one burning He above a degenerate C-O core and another burning H, below a deep convective envelope. In between lies the intershell region composed mostly of ${}^4\text{He}$. The He-burning shell is thermally unstable, flashing every 10^4 years or so. The energy produced by the thermal pulse (TP) drives a convective pocket in the He-intershell which acts to homogenize abundances within that region. After the occurrence of a TP the convective envelope may move inwards and mix products of partial He-burning (mostly ${}^4\text{He}$ left unburnt and ${}^{12}\text{C}$, see Fig. 1) from the core to the stellar surface. This is the third dredge-up (TDU), and is the mechanism responsible for turning (single) stars into C stars, where $\text{C}/\text{O} > 1$ in the surface layers. The TDU also mixes heavy elements produced by the s process from the He-shell to the surface, where they were created during the previous interpulse [8]. Following dredge-up, the star contracts, the H-shell is re-ignited and the star enters the interpulse phase where H-burning provides most of the luminosity.

Hot bottom burning (HBB) can occur for stars with $m \geq 4M_{\odot}$, when the base of the convective envelope dips into the top of the H-shell resulting in a thin layer hot

enough to sustain proton-capture nucleosynthesis. Observational evidence for HBB includes the lack of bright C-rich AGB stars in the Large and Small Magellanic Clouds (LMC and SMC) [22]; many of these stars are also rich in Li and *s* process elements. HBB converts ^{12}C into ^{14}N and will prevent the atmosphere from becoming C rich [4]. The copious amounts of ^{14}N produced in this case will be primary¹ owing to the primary ^{12}C being dredged from the He-shell. Intermediate-mass evolution is sensitive to the initial composition and the mass-loss law used in the calculation [7], where the minimum stellar mass for HBB is pushed to lower mass in lower metallicity models.

There is evidence from AGB stellar spectra [1], and from pre-solar grains [18] that “extra-mixing” processes are also operating in low-mass ($m \leq 2M_{\odot}$) AGB stars, along with the TDU. The physical mechanism(s) responsible for the extra mixing are not known, although various processes have been proposed including rotation and thermohaline mixing. The presence of a binary companion could have dramatic consequences for the evolution and nucleosynthesis, however I leave discussions to Izzard, Taam and Podsiadlowski (these proceedings).

3 Synthetic versus detailed AGB models

Owing to fact that calculating a TP-AGB model is a computationally intensive task, synthetic AGB models, which use fitting formulae to model the evolution quickly, have proved to be a successful approach for population syntheses studies that require $N \sim 10^6$ stars. Historically this approach was validated by the fact that the stellar luminosity on the AGB is nearly a linear function of the core mass [19, 9], although this relation breaks down for stars undergoing HBB [2]. Synthetic AGB models have successfully been used to model AGB populations [9], and compute stellar yields [23, 17, 12].

Many of the parameterizations used in synthetic evolution studies are derived from detailed stellar models, such as the growth of the H-exhausted core with time, and as such are only accurate over the range in mass and metallicity of the stellar models they are based upon. An example is provided by [23] who compute AGB yields for initial masses between 0.9 and $8M_{\odot}$ whereas the interpulse-period-core mass relation [3] they use was only derived for stars with initial masses between 1 and $3M_{\odot}$. What effect this has on the yields is unclear since this relation will affect the number of TPs during the TP-AGB phase and hence the level of chemical enrichment. Recent improvements in computer power mean that grids of detailed AGB models can now be produced in a reasonable time [13, 14, 10]; however producing yields from $N \geq 20$ AGB stars for any given metallicity range is still challenging. For this reason synthetic models are still preferred for some applications.

An example of the difference between detailed models and the fits used in synthetic AGB algorithms is shown in Fig. 2 for the interpulse-period core mass relation. We show results from detailed AGB models of solar composition against two commonly used fits. The fits are a reasonable match to the detailed models with small core masses ($M_c \leq 0.7M_{\odot}$), but under-estimate the growth of the interpulse period for larger core masses.

¹ produced from the H and ^4He initially present in the star.

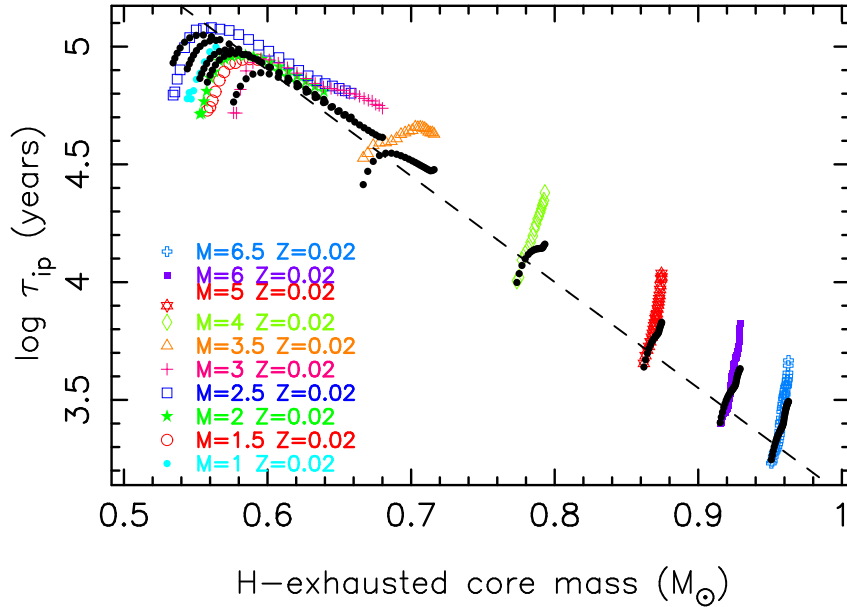


Fig. 2. Interpulse period ($\log \tau_{\text{ip}}$ years) as a function of core mass (M_{\odot}) for the $Z = 0.02$ stellar models (colored dots). The fits from [3] (dashed line) and [21] (solid black dots) are shown for comparison.

4 The stellar yields from single AGB models

In [15] we present results from grids of AGB models, including data about the stellar structure and the yields. These are also available for download from:

http://www.mso.anu.edu.au/~akarakas/model_data/

and

http://www.mso.anu.edu.au/~akarakas/stellar_yields/

More details about the numerical technique and the yields can be found in [15], but we note here that yield can be negative, in the case where the element is destroyed, and positive if it is produced.

In Fig. 3 we show the AGB yields of ^{12}C as a function of the initial stellar mass. The yields have been weighted by the initial mass function (IMF) of [16], and we show results from the $Z = 0.02$ (solar), 0.008 (LMC) and 0.004 (SMC) metallicity models. For comparison we also show the yields from a number of different synthetic AGB calculations, and from [25]; see the figure caption for details. The yield of ^{12}C is representative of low-mass AGB nucleosynthesis where the main contributor to the yield is either the FDU at low mass ($m \leq 1.2M_{\odot}$), where the ^{12}C surface abundance decreases, or from the TDU where we find substantial increases. Models with $m > 4M_{\odot}$ produce little ^{12}C at these metallicities owing to HBB. The yields of ^{14}N instead peak in this mass range, even after weighting the yields with an IMF [15]. HBB may also produce ^{23}Na , ^{26}Al and the heavy Mg isotopes through the combined operation of the TDU and the MgAl chains [13, 14].

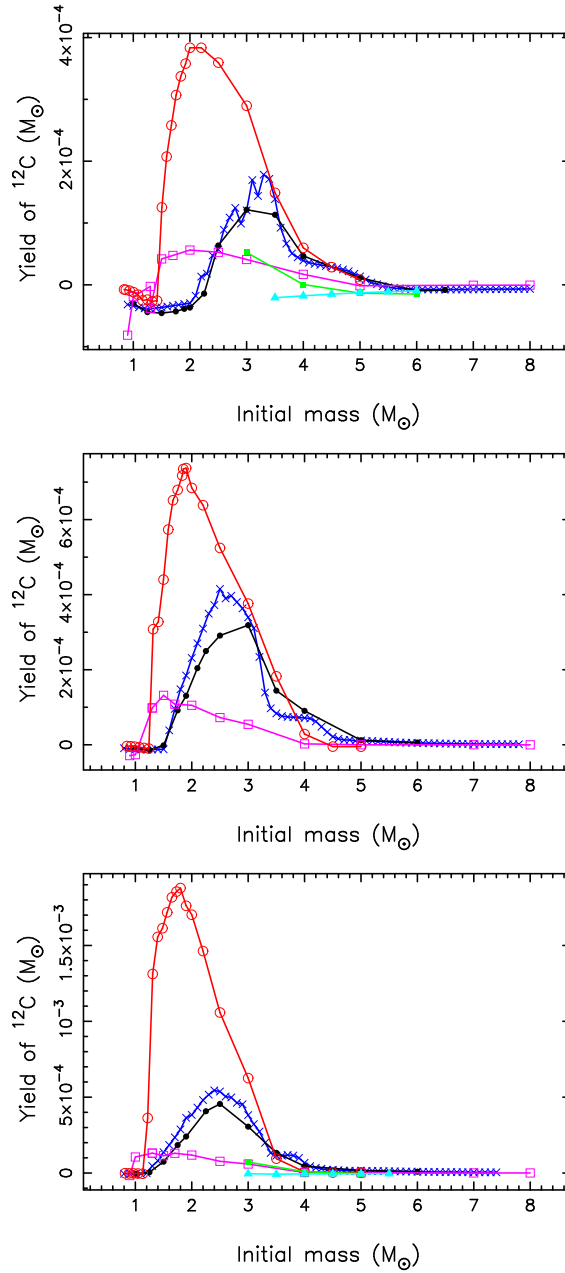


Fig. 3. Weighted yield of ^{12}C as a function of the initial mass for the $Z = 0.02$ (top), the $Z = 0.008$ (middle) and the $Z = 0.004$ models (bottom). We show results from our calculations (black solid points), [23] (open magenta squares), [6] (solid green squares), [17] (open red circles), [25] (solid aqua triangles) and [12] (blue crosses). [6] and [25] do not provide yields for $Z = 0.008$ and cover a narrower mass range, between 2.5 and $6M_{\odot}$.

Our yields are similar in behavior to those of [17], although because her models have deeper TDU at a lower core mass, the yields of He-shell material e.g. ^4He , ^{12}C are higher. We notice significant differences with [23] especially in regards to ^{14}N . This is owing to their simplistic treatment of HBB nucleosynthesis which underpredicts the amount of CNO cycling compared to all other computations. The yields from [23] for masses between ~ 6 to $8M_{\odot}$ are based on extrapolations of fitting formula to this mass range and should be treated with caution. Their models also produce much more ^{16}O at $m \sim 1M_{\odot}$ at $Z = 0.02$; this is especially noticeable when weighting by the IMF. This was also found by [12] and the reasons for the production are unclear because the FDU should not enhance the surface in ^{16}O .

In Fig. 4 we show the yields of ^{15}N and ^{17}O as a function of initial mass and metallicity. The unexpected result is the production of ^{15}N in the lowest Z AGB models; this is owing to leakage from the $^{14}\text{N}(p,\gamma)^{15}\text{O}$ reaction at very high temperature. For the ^{15}N yields from the more metal-rich models, and for ^{17}O , the yields scale with Z as expected. Fig. 4 shows that low-mass AGB stars can equally participate in the production of ^{17}O , whereas this has been previously ignored in chemical evolution studies e.g. [20] probably owing to a lack of available yields.

4.1 Yields for planetary nebulae

Table 1. PN yields $3M_{\odot}$, $Z = 0.02$ model.

Isotope	A	yield	$X0(i)$	$\langle X(i) \rangle$	$N(i)/N(H)$
^4He	4	4.39725E-02	2.92881E-01	3.21630E-01	1.23369E-01
^{12}C	12	1.10031E-02	3.40894E-03	1.06028E-02	1.35560E-03
^{13}C	13	7.72216E-05	4.10914E-05	9.15790E-05	1.08084E-05
^{14}N	14	2.23653E-03	1.05449E-03	2.51674E-03	2.75816E-04
^{15}N	15	-3.12235E-06	4.14117E-06	2.09975E-06	2.14776E-07
^{16}O	16	-8.21213E-04	9.60272E-03	9.06575E-03	8.69348E-04
^{17}O	17	3.40679E-05	3.87707E-06	2.61507E-05	2.36017E-06
^{18}O	18	-8.87124E-06	2.16060E-05	1.58060E-05	1.34728E-06

In [15] we present yields for PN, where we integrate the amount of matter lost over the last two TPs. In Table 1 we show an example of the yields for a $3M_{\odot}$ progenitor of solar composition. The columns contain the species i , the atomic weight $A(i)$, followed by the net yield (in M_{\odot} ; see [15] for the definition), the average mass fraction of i lost in the wind from the last two TPs, $\langle X(i) \rangle$, and the initial mass fraction $X0(i)$. The final column is the abundance of i by number compared to the number of hydrogen atoms, N_i/N_H , in the matter lost over the final two TPs. The online tables include yields for all 74 species included in the nuclear network.

These yields can be directly compared to the composition of PNe and as such could be useful for comparisons to objects in the Galaxy, LMC and SMC. This is because the initial C, N and O abundances used in the stellar models were taken from abundances derived from HII regions of the Magellanic Clouds, see [15] for details.

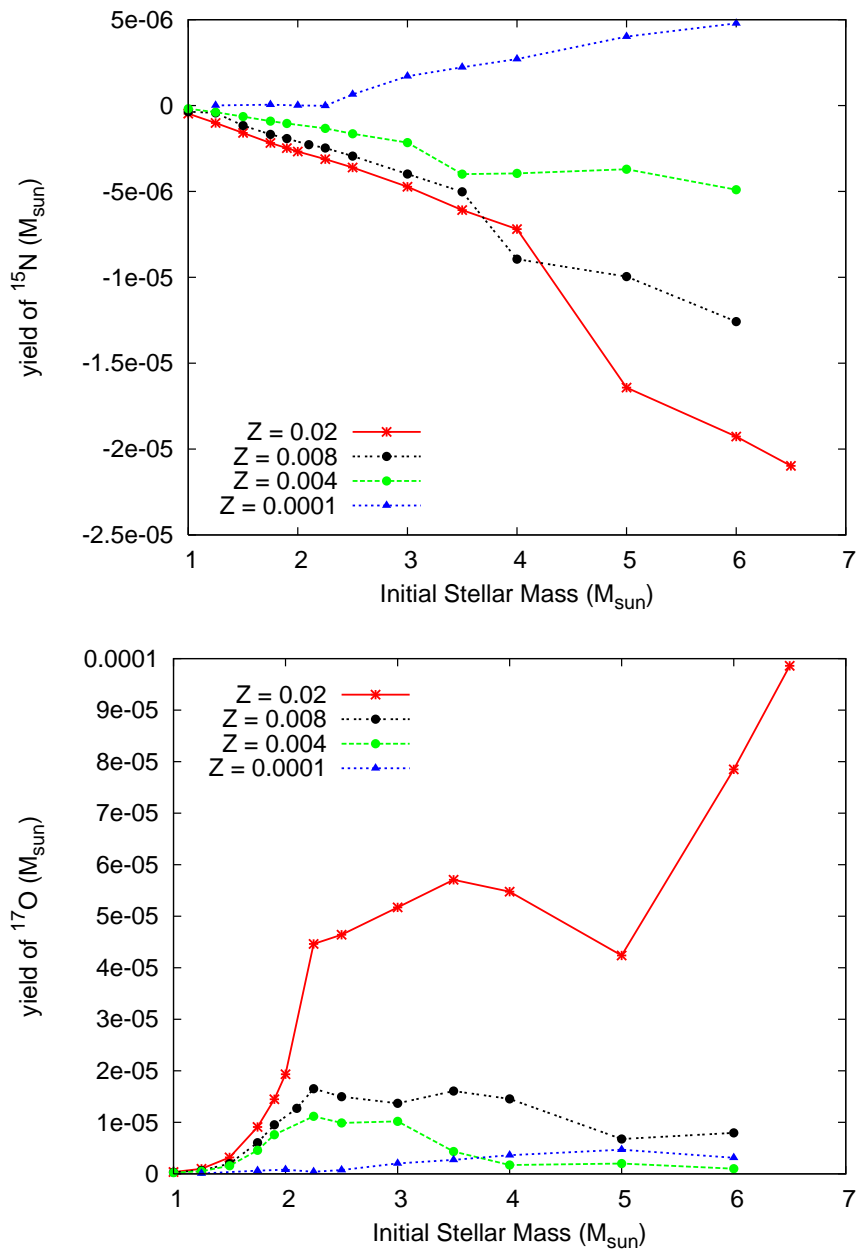


Fig. 4. Yield of ^{15}N (top panel) and ^{17}O (lower panel) as a function of the initial mass and metallicity.

References

1. Abia, C. & Isern, J. 1997, *MNRAS*, 289, L11
2. Bloeker, T. & Schoenberner, D. 1991, *A&A*, 244, L43
3. Boothroyd, A. I. & Sackmann, I.-J. 1988, *ApJ*, 328, 653
4. Boothroyd, A. I., Sackmann, I.-J., & Ahern, S. C. 1993, *ApJ*, 416, 762
5. Busso, M., Gallino, R., & Wasserburg, G. J. 1999, *ARA&A*, 37, 239
6. Forestini, M. & Charbonnel, C. 1997, *A&AS*, 123, 241
7. Frost, C. A., et al. 1998, *A&A*, 332, L17
8. Gallino, R., et al. 1998, *ApJ*, 497, 388
9. Groenewegen, M. A. T. & de Jong, T. 1993, *A&A*, 267, 410
10. Herwig, F. 2004, *ApJS*, 155, 651
11. Herwig, F. 2005, *ARA&A*, 43, 435
12. Izzard, R. G., et al. 2004, *MNRAS*, 350, 407
13. Karakas, A. I. & Lattanzio, J. C. 2003, *PASA*, 20, 279
14. Karakas, A. I., et al. 2006, *ApJ*, 643, 471
15. Karakas, A. I. & Lattanzio, J. C. 2007, *PASA*, submitted
16. Kroupa, P., Tout, C. A., & Gilmore, G. 1993, *MNRAS*, 262, 545
17. Marigo, P. 2001, *A&A*, 370, 194
18. Nollett, K. M., Busso, M., & Wasserburg, G. J. 2003, *ApJ*, 582, 1036
19. Paczynski, B. 1975, *ApJ*, 202, 558
20. Romano, D. & Matteucci, F. 2003, *MNRAS*, 342, 185
21. Wagenhuber, J. & Groenewegen, M. A. T. 1998, *A&A*, 340, 183
22. Wood, P. R., Bessell, M. S., & Fox, M. W. 1983, *ApJ*, 272, 99
23. van den Hoek, L. B. & Groenewegen, M. A. T. 1997, *A&AS*, 123, 305
24. van Winckel, H. 2003, *ARA&A*, 41, 391
25. Ventura, P., D'Antona, F., & Mazzitelli, I. 2002, *A&A*, 393, 215